Nonlinearity Tolerant High-speed DMT Transmission with 1.5-μm Single-mode VCSEL and Multi-core Fibers for Optical Interconnects

Lu Zhang, Joris Van Kerrebrouck, *Student Member, IEEE,* Rui Lin, Xiaodan Pang, *Member, IEEE,* Aleksejs Udalcovs, *Member, IEEE,* Oskars Ozolins, *Member, IEEE,* Silvia Spiga, Markus-Christian Amann, *Fellow, IEEE,* Geert Van Steenberge, Lin Gan, Ming Tang, *Senior Member, IEEE,* Songnian Fu, Richard Schatz, Sergei Popov, Deming Liu, Weijun Tong, Shilin Xiao, Guy Torfs, *Member, IEEE,* Jiajia Chen, *Senior Member, IEEE,* Johan Bauwelinck, *Member, IEEE,* and Xin Yin, *Member, IEEE*

***Abstract*— We experimentally demonstrate the generation of 107-Gbit/s net-rate optical discrete multitone (DMT) signal using a 1.5-μm single-mode vertical cavity surface emitting laser (VCSEL) with modulation bandwidth of 22-GHz. Utilizing a nonlinearity-tolerant channel equalization algorithm for digital signal processing (DSP), total net-rates of 726.6-Gbit/s over 2.5-km dispersion-uncompensated 7-core fiber and 533.1-Gbit/s over 10-km dispersion-compensated 7-core fiber below 7% overhead hard-decision forward error correction (HD-FEC) limit have been experimentally achieved with a 1.5-μm VCSEL based intensity-modulation direct-detection (IM/DD) system. The features of the 1.5-μm single-mode VCSEL, 2.5-km/10km multi-core fibers and fan-in/fan-out modules are presented. Besides, the Volterra series-based nonlinearity-tolerant channel equalization algorithm, which improves the signal-to-noise ratio (SNR) with more than 5-dB, is mathematically described and experimentally validated. The results have demonstrated that 1.5-μm single-mode VCSEL and multi-core-fiber-based transmission can be a promising candidate to solve the capacity challenges in short-reach optical interconnects.**

***Index Terms*— Vertical cavity surface emitting laser (VCSEL), discrete multitone (DMT), multi-core fiber (MCF), digital signal processing (DSP), Volterra series model, nonlinearity-tolerant channel equalization.**

I. Introduction

With the massive deployment of novel Internet applications, the high capacity requirements have put a great pressure on datacenter networks. According to the prediction from *Cisco Ltd.* [1], most of the datacenter traffic will stay within the mega datacenters and high data rate short-reach interconnections are highly demanded especially for intra-datacenter networks. According to [2], the data rate per channel will improve from 25-Gbit/s to 100-Gbit/s or even higher for next generation Ethernet interfaces in intra-datacenter networks, and the total data rate of the interface is expected to be 400-Gbit/s or even higher. As a result, optical fiber communication is considered as an attractive technology to solve this capacity bottleneck [1]. Moreover, to meet the ever-increasing capacity requirements while keeping a low deployment cost, optical intensity-modulation direct-detection (IM/DD) system are preferred thanks to its low system cost.

Among the methods proposed to realize the high capacity and low-cost datacenter interconnects, vertical cavity surface emitting laser (VCSEL) based optical links together with advanced modulation formats are recognized as a promising

Manuscript received xx xx, 2018; This work was partly supported by the Natural Science Foundation of China (#61331010, 61722108, 61775137, 61671212, and 61550110240), H2020 5GPPP 5G-PHOS research program (grant 761989), European Commission through the FP7 project MIRAGE (ref.318228), Swedish Research Council (VR), the Swedish Foundation for Strategic Research (SSF), Göran Gustafsson Foundation, Swedish ICT-TNG, the Celtic-Plus sub-project SENDATE-EXTEND & SENDATE FICUS funded by Vinnova. (*Lu Zhang and Joris Van Kerrebrouck contributed equally to this work*, corresponding authors: Jiajia Chen, Xin Yin)

L. Zhang is with the State Key Laboratory of Advanced Optical Communication System and Networks, Shanghai Jiao Tong University, Shanghai 200240, China; and also with KTH Royal Institute of Technology, Kista 164 40, Sweden (emails: luzhang_sjtu@sjtu.edu.cn; lu8@kth.se).

J. Van Kerrebrouck, G. Torfs, J. Bauwelinck, and X. Yin are with Ghent University - imec, IDLab, Department of Information Technology, Gent 9000, Belgium (e-mails: joris.vankerrebrouck@ugent.be; guy.torfs@ugent.be; johan.bauwelinck@ugent.be; xin.yin@ugent.be).

R. Lin, X. Pang, R. Schatz, U. Westergren, S. Popov are with KTH Royal Institute of Technology, Kista 164 40, Sweden (e-mails: rulin@kth.se; xidaodan@kth.se; rschatz@kth.se; urban@kth.se; sergeip@kth.se; jiajiac@kth.se).

J. Chen is with MOE International Laboratory for Optical Information Technologies, South China Academy of Advanced Optoelectronics, South China Normal University, Guangzhou 510006, China, and KTH Royal Institute of Technology, Kista 164 40, Sweden (e-mail: jiajiac@kth.se)

A. Udalcovs and O. Ozolins are with the NETLAB, RISE Acreo AB, Kista SE-164 25, Sweden (e-mails: aleksejs.udalcovs@ri.se; oskars.ozolins@ri.se).

R. Lin, L. Gan, M. Tang, S. Fu and D. Liu are with the Wuhan National lab for Optoelectronics (WNLO), Huazhong University of Sci&Tech (HUST), Wuhan 430074, China (e-mails: lingan@hust.edu.cn; tangming@hust.edu.cn; songnian@mail.hust.edu.cn; dmliu@hust.edu.cn).

S. Spiga and M. C. Amann are with the Walter Schottky Institut, Technische Universität München Garching 85748, Germany (e-mails: silvia.spiga@wsi.tum.de; amann@wsi.tum.de).

G. Van Steenberge is with the Centre for Microsystems Technology, Ghent University-imec, Ghent 9052, Belgium (e-mail: geert.vansteenberge@ugent.be).

W. Tong is with the Yangtze Optical Fibre and Cable Company Ltd (YOFC), Wuhan 430073, China (e-mail: tongweijun@yofc.com).

S. Xiao is with the State Key Laboratory of Advanced Optical Communication System and Networks, Shanghai Jiao Tong University, Shanghai 200240, China (e-mail: slxiao@sjtu.edu.cn).

candidate thanks to their high spectrum efficiency, low power consumption and ease of integration into VCSEL arrays [3]. 100-Gbit/s short-reach interconnects have been experimentally demonstrated employing short-wavelength VCSELs and multimode fibers (MMF), together with advanced modulation formats, such as pulse amplitude modulation (PAM), discrete multitone (DMT), or carrier-less amplitude and phase modulation (CAP) [4-8]. However, the MMF transmission distance is limited, up to a few hundred meters. To the best of our knowledge, the longest transmission distance is 550-m MMF with 106-Gbit/s net-rate per channel [8] at hard-decision forward error correction (HD-FEC) limit. Meanwhile, long-wavelength (LW, e.g. 1.5-μm) and single-mode (SM) VCSELs have gained increasing interests thanks to the lower power consumption, low transmission loss in silica-based optical fibers and compatibility with mature dense wavelength division multiplexing (DWDM) devices [9], which is desired in the long term to support future Terabit and beyond interconnects in a mega-datacenter. Several research works achieving high data rates with LW VCSELs have been reported [10-13]. In [10], a 74.8-Gbit/s net-rate LW SM-VCSEL link is demonstrated with real-time 3-level electrical duo-binary modulation. [11] achieves 87.5-Gbit/s net-rate over 0.5-km standard single mode fiber (SSMF) (79.2-Gbit/s over 4 km SSMF) at 20% overhead HD-FEC with a 1.5-μm VCSEL and DMT modulation. In [12], 81.6-Gbit/s net-rate PAM-4 transmission is demonstrated over 1.6-km SSMF with a 1525-nm SM-VCSEL. Besides, [13] reports a 56-Gbit/s net-rate DMT transmission over 12-km SSMF. Nevertheless, the IM/DD system using cost-effective and high-speed LW SM-VCSEL to reach 100-Gbit/s net-rate per lane is still challenging even for short-reach communications.

Meanwhile, spatial division multiplexing (SDM) is widely recognized as a key enabling technology to increase bandwidth-density for optical interconnects [14]. The current datacenter network using either individual fibers or fiber ribbons are costly, bulky, hard to manage and not scalable. Such issues can be addressed by introducing multi-core fiber (MCF) based SDM transmission. Therefore, the use of VCSELs and MCF to realize multichannel transmission is a promising solution for cost- and energy-effective high-speed optical interconnects [15].

This paper is an extension of [16] providing further analyses. In this paper, we significantly extend the previous work by: 1) elaborating the features of key components including the 1.5-μm SM-VCSEL, MCFs and fan-in/fan-out modules; 2) introducing theoretical derivations of the nonlinearity tolerant digital signal processing (DSP) flow; 3) showing the DSP flow optimization process with experiments; 4) extending the results with 10-km 7-core MCF transmission. In the experiments, we have demonstrated the generation of optical DMT signal of 107-Gbit/s net-rate (gross 114-Gbit/s), using a 1.5-μm SM-VCSEL with direct modulation bandwidth of 22-GHz. To overcome the nonlinearities that come from the VCSEL and the optical link, we have utilized a nonlinearity tolerant DSP flow to improve the transmission performance. The experimental results show that, after 2.5-km dispersion-uncompensated 7-core MCF optical DMT transmission, the maximal achieved core net-rate is 105-Gbit/s (gross 112.3-Gbit/s when cyclic prefix overhead and channel equalization pilot overhead have been considered) and the total net-rate is 726.6-Gbit/s (gross 777.5-Gbit/s). After 10-km dispersion-compensated 7-core MCF, the maximum achieved core net-rate is 83.1-Gbit/s (gross 88.9-Gbit/s) and the total net-rate is 533.1-Gbit/s (gross 570.5-Gbit/s). To the best of our knowledge, this is the highest DMT net-rate ever achieved by means of LW SM-VCSEL technology.

The remainder of this paper is structured as follows: Section II shows the operational principles including the features of LW SM-VCSEL, 7-core MCFs, fan-in/fan-out modules and nonlinearity tolerant DSP flow. Section III shows the experimental setup and Section IV shows the system optimization and MCF transmission performance.

II. Operational Principles

High-speed optical short reach interconnects need careful design of the optical devices, transmission link and DSP flow. In section II-A, the feature of the 1.5-μm SM-VCSEL is presented. In section II-B, the feature of the 7-core MCFs and the fan-in/fan-out modules are depicted. In section II-C, the mathematical derivation of the nonlinearity tolerant DSP flow is provided.

A. 1.5-μm Single Mode VCSEL

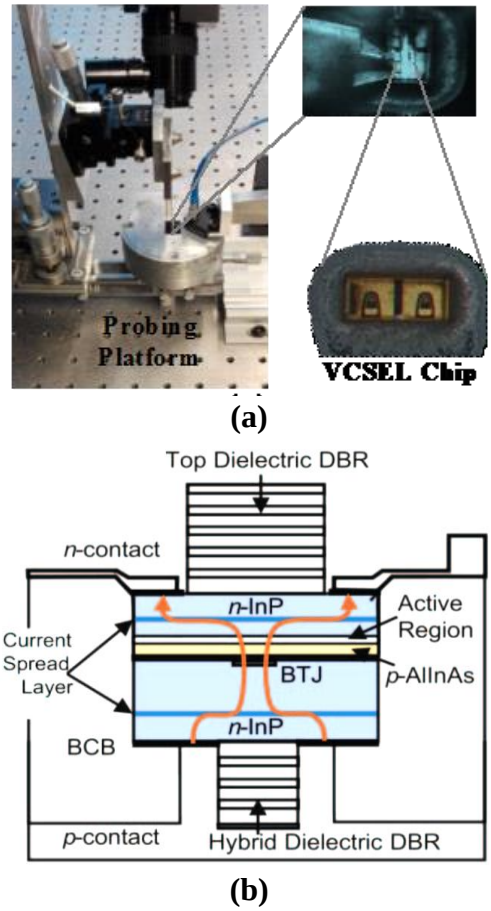

Fig. 1. (a) The experimental probing setup and (b) the VCSEL structure.

The experimental probing platform setup and the VCSEL structure are shown in Fig. 1 (a) and Fig. 1 (b), respectively. The VCSEL die is electrically driven via a 100-μm GSG 50-GHz probe. The light generated in the VCSEL is coupled into a single-mode lens fiber. There was no temperature controller (TEC) used in the setup. This 1.5-μm SM InP-based VCSEL uses an ultra-short semiconductor cavity (~1.5-μm) and two distributed Bragg reflectors (DBRs) to enhance its bandwidth [9]. The optical gain is provided by an active region with seven AlGaInAs quantum wells and current confinement is achieved by a p+ –AlGaInAs/n+ –GaInAs buried tunnel junction (BTJ) of 4-μm. The reduced cavity length allows the operator to minimize the photon lifetime by maintaining single-mode operation, and an involved doping profile has been used to overcome parasitic limitations and thermal issues. The particular VCSEL used in the experiments is a 1541.2-nm laser, with a maximum optical output power after probing of 1-dBm. The VCSEL is optimized for a 50-Ω impedance to minimize reflection.

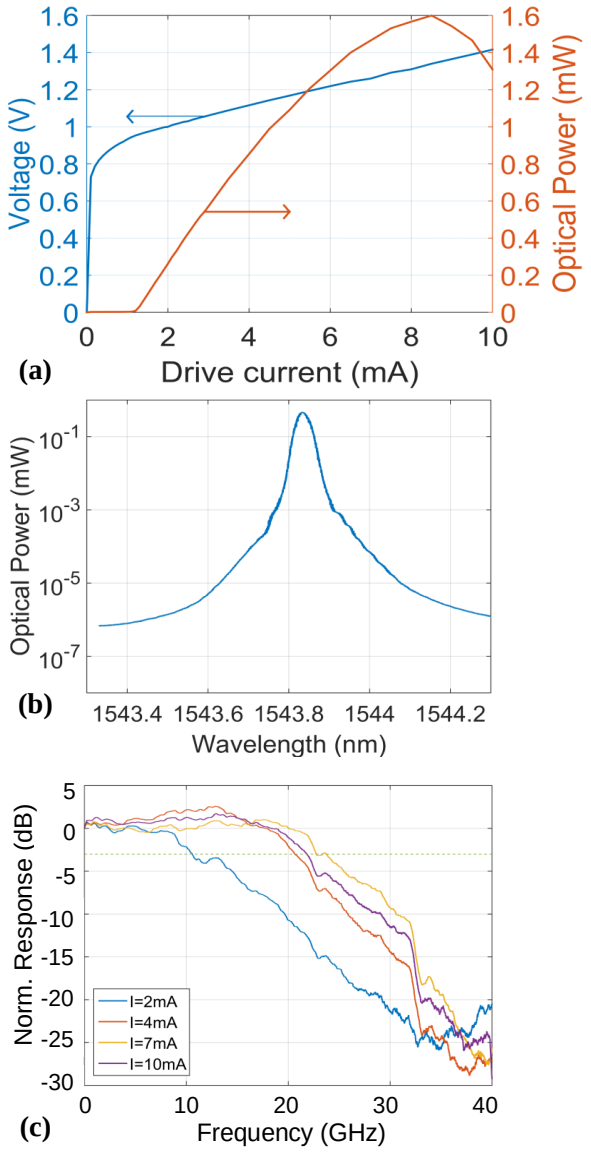

Fig. 2. (a) The P-I-V curves, (b) optical spectrum and (c) small-signal S_{21} responses of VCSEL.

Fig. 2 (a) shows the measured P-I-V curves of the VCSEL. This 1.5-μm SM-VCSEL shows an impedance of 54-Ω at 10-MHz and 63-Ω at 10-GHz. The threshold current is ~1.5-mA, and the maximum optical output power is at ~8-mA. With a VCSEL current larger than 8-mA, the optical power decreases due to thermal heating of the VCSEL. The optical spectrum is shown in Fig. 2 (b), measured at a bias current of 7-mA. Fig. 2 (c) presents the small-signal S_{21} responses of the electrical–optical–electrical conversion. The maximum bandwidth of 22-GHz and an optimum flat response is reached with a bias current of around 7~8-mA, where however the VCSEL optical output power starts to degrade due to thermal heating. More properties and design principles of the 1.5-μm SM-VCSEL can be found in [9].

B. 7-core MCFs and Fan-in/Fan-out Modules

In the experiments, we have adopted 2.5-km 7-core MCF and 10-km 7-core MCF for demonstration of high-speed optical links. The cross-section view of the 2.5-km 7-core MCF used for our experiments is shown in Fig. 3 (a). The stack and draw process is applied to fabricate 7-core homogeneous MCFs, and therefore, the properties of different cores are almost the same. The MCF is designed for short-reach communications with ultra-low crosstalk [17,18]. The cladding diameter of the MCF is 150-μm and the average core pitch is 41.5-μm, respectively. The crosstalk between adjacent cores is suppressed to be as low as −45dB/100km. The attenuation loss is less than 0.2-dB/km at 1.5-μm and the chromatic dispersion of the MCF is 17.1-ps/nm/km.

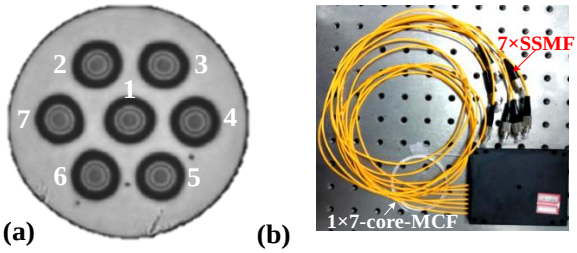

Fig. 3. (a) The cross-section view of the 2.5-km 7-core MCF and (b) the fabricated fan-in/fan-out module.

The low-loss and reliable connectivity between MCF and SSMFs is also of great importance for the MCF based optical links by using fan-in/fan-out modules. The fabricated fan-in/fan-out module is shown in Fig. 3 (b). In the development of fan-in/fan-out modules, we have developed proprietary technology [17] of chemical etching to reduce the length of transition region sharply and to keep a uniform etched diameter long enough for fiber bundle fabrication. The crosstalk between adjacent cores in the fan-in/fan-out modules is measured to be less than -50dB. The insertion loss per fan-in/fan-out is less than 1.5 dB.

C. Nonlinearity-tolerant DSP Flow

Although VCSEL presents an attractive solution for high data-rate, cost-effective and energy-efficient optical links, the VCSEL can exhibit nonlinear behaviors, especially for high bias currents, due to the internal heating [19]. Moreover, the DMT signals have a large dynamic range because of the high

peak-to-average ratio (PAPR), which making them more vulnerable to nonlinearities. Besides the modulation nonlinearities of VCSELs, the nonlinearities of the short-reach DMT optical link also come from other sources, such as inter-subcarrier mixing in square-law detection of photo detector, and electrical amplifiers due to the high PAPR of the DMT signal.

To mitigate such detrimental effects from system nonlinearities, a nonlinearity-tolerant DSP flow for optical DMT transmission in VCSEL based short reach optical link is required. The DSP flow of the transmitter and the receiver in our system is shown in Fig. 4.

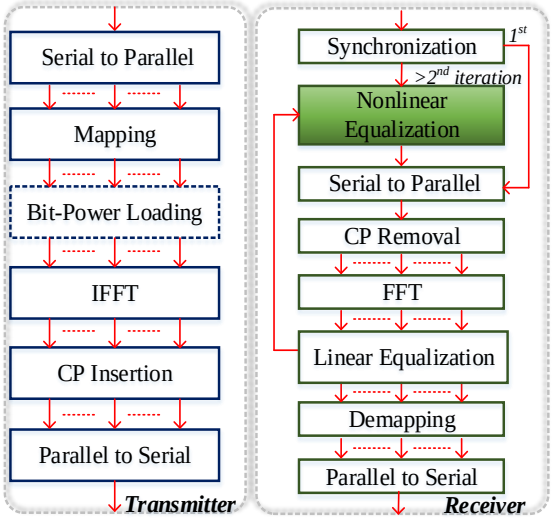

Fig. 4. DSP flow of the transmitter and the receiver

Except for the channel equalization, the DSP flow is similar to a conventional DMT system. In the transmitter, a mapping module is used to transform the binary data in different subcarriers to QAM symbols. Meanwhile, the bits and power loading with Chow algorithm [20] is utilized at the transmitter to enhance the capacity of the DMT system with the spectrally shaped (always low-pass filtering property) channels. After mapping, the inverse fast Fourier transform (IFFT) module transforms the frequency domain symbols into time domain to realize the DMT modulation. Then, cyclic prefix (CP) is inserted to reduce the influence of inter-symbol interference. At the receiver, the DSP flow after synchronization corresponds to the reversed process of the transmitter DSP flow, except the channel equalization.

The channel equalization is composed of linear equalization (LE) and nonlinear equalization (NE). First, the signal after the FFT module passes through the pilot based one-tap LE, which is used to compensate the fiber chromatic dispersion and to reduce the system additive Gaussian noise influence [21]. We assume that $P(m,l)$ represents the pilot carried with subcarrier index m at the i-th symbol, $P'(m,l)$ represents the corresponding received pilot. The number of pilots is N_p, and the estimation of the linear channel response at the m-th subcarrier is expressed as:

$$H(m) = \left(\sum_{l=1}^{N_p} P'(m,l)/P(m,l)\right)/N_p \,. \tag{1}$$

The number of the total DMT symbols is denoted as N_s, and the index l of the pilots corresponds to:

$$l = (k-1)\cdot N_s / N_p + 1, \quad k = 1,\ldots, N_p \,. \tag{2}$$

After LE, the signal is equalized with $H(m)$. Assuming that $R(m, l)$ represents the received data with subcarrier index m at the i-th symbol, the data $Y(m,l)$ after LE is expressed as:

$$Y(m,l) = R(m,l)/H(m) \,. \tag{3}$$

After LE, $Y(m, l)$ is equalized with a nonlinear equalizer. Here, a simplified Volterra series nonlinear model [22, 23] is used for estimating the nonlinearity components, which considers only the 2nd-order and partially the 3rd-order terms. In time domain, the transmission model is expressed as follows:

$$\begin{aligned} r(n) = w + & \sum_{i=0}^{M_1-1} h_1(i)x(n-i) + \\ & \sum_{i=0}^{M_2-1}\sum_{j=i}^{M_2-1} h_2(i,j)x(n-i)x(n-j) + \\ & \sum_{i=0}^{M_3-1}\sum_{j=i}^{M_3-1}\sum_{k=j}^{M_3-1} h_3(i,j,k)x(n-i)x(n-j)x(n-k) + \ldots . \end{aligned} \tag{4}$$

where n is the index of time domain samples, $x(n)$ is the transmitted DMT signal, w is the additive Gaussian noise originating from the device background noise and channel impairments, $h_K(\ldots)$ (K>0) is the K-th order Volterra kernel corresponding to the linear (K=1) or nonlinear (K>1) channel responses, and M_K is the memory length of K-th order effect. Since linear distortions (w and h_1) have been well compensated with a low complexity and low overhead [21] LE in (3), we only consider h_2 and h_3 in (4) for nonlinear compensation. The nonlinear compensation is an iterative process. At the first iteration, $Y(m, l)$ is fed to a decision-feedback module followed by a IFFT re-modulation module to estimate the transmitted DMT samples $x(n)$, which are denoted as $x'(n)$. Then, the nonlinear kernels are estimated [23] by a recursive least square (RLS) algorithm using the training symbols.

After obtaining the nonlinear kernels with the RLS algorithm and training symbols, the signal with nonlinear distortions is equalized by subtracting the nonlinear noise using (5) with estimated h'.

$$\begin{aligned} y'(n) = y(n) - & \sum_{i=0}^{M_2-1}\sum_{j=i}^{M_2-1} h_2'(i,j)x'(n+\alpha-i)x'(n+\alpha-j) - \\ & \sum_{i=0}^{M_3-1}\sum_{j=i}^{M_3-1}\sum_{k=j}^{M_3-1} h_3'(i,j,k)x'(n+\alpha-i)x'(n+\alpha-j)x'(n+\alpha-k) \end{aligned} \tag{5}$$

The delay factor α of the nonlinear equalizer is inserted to change the position of the reference taps in (5). After equalization with (5), $y'(n)$ is utilized as the input for decision-feedback module for the next iteration until the loop comes to the predefined iteration loop number.

III. Experimental Setup

The experimental setup is shown in Fig. 5. In the experiments, the length of the IFFT and CP are set to 1024 and 16, respectively, and the first subcarrier was set to null. The binary sequence used to generate the DMT symbols is random sequence generated from *MATLAB* software. There are 140 DMT symbols generated for transmission. The generated DMT

signal has a PAPR of ~ 11-dB. For simplicity in the DSP implementation, the memory length M_2 and M_3 of NE are kept equal. The VCSEL bias current is set to 7.8-mA as a trade-off between bandwidth, linearity and output optical power. There is no temperature controller (TEC) used in the setup. The measured central wavelength of the probed VCSEL is 1543.2-nm and the captured output optical power is 1-dBm.

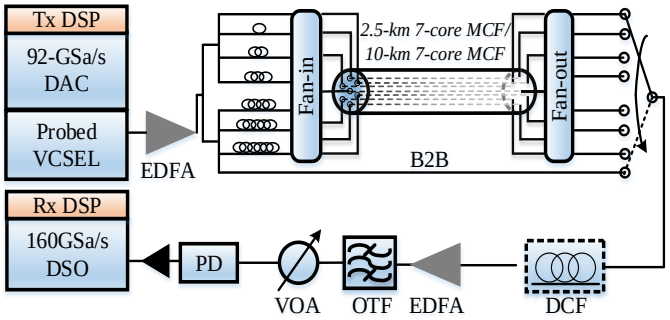

Fig. 5. Experimental setup

The DMT signals are generated with *MATLAB* software and loaded into a 92-GSa/s digital to analog converter (DAC, Keysight AWG M8196A, 3-dB bandwidth 32-GHz). The output amplitude of the DAC is 720-mV (peak-to-peak voltage). The clipping ratio at the transmitter is set to 0.7 to improve the output signal-to-noise ratio (SNR) from the DAC. The signal from the directly modulated VCSEL is fed into a booster Erbium-doped fiber amplifier (EDFA) with fixed output power of 14.8-dBm to compensate the insertion loss of optical coupler. The signal is split in a fan-in module of a 2.5-km 7-core MCF or a fan-in module of a 10-km 7-core MCF, using one 1:2 optical coupler cascaded with two 1:4 optical couplers, where the last port is used for optical back-to-back (B2B) measurements. The optical delay lines (0.5 to 10 meters) are used to de-correlate the signals to emulate a practical system using seven independently modulated VCSELs. After the MCF transmission, the signals are detected individually after a fan-out module. No any dispersion compensation fiber (DCF) is used after the 2.5-km 7-core MCF transmission, while a fixed DCF (-159 ps/nm) is employed after the 10-km 7-core MCF. The signal is amplified by an EDFA for pre-amplification since the sensitivity of the employed PIN is low. An optical tunable filter (OTF) is utilized to filter out the amplified spontaneous emission (ASE) noise. A 90-GHz PIN photo-detector (PD, sensitivity: 0.5-A/W) is used at the receiver. A variable optical attenuator (VOA) is used before the PD for bit error rate (BER) curves. The electrical signal resulting from this direct-detection is amplified by a 65-GHz linear electrical amplifier with 11-dB gain and captured by a 160-GSa/s digital storage oscilloscope (DSO, 3-dB bandwidth 63-GHz).

The measured system response with optical B2B, 2.5-km 7-core MCF and 10-km 7-core MCF are shown in Fig. 6. Here, the best (highest 3-dB bandwidth) and the worst (lowest 3-dB bandwidth) cores are shown. The response for 10-km 7-core MCF based system is equipped with DCF. It can be observed that the B2B and 10-km MCF cases are low-pass filtering channels with more than 10-dB attenuation within 30-GHz. The low-pass filtering property of optical B2B case is caused by the VCSEL response the chirps of the VCSEL. Besides, the low-pass filtering property of 10-km MCF case is also caused by partial chromatic dispersion compensation from DCF. Thus, bit-power loading can help improve the system capacity and spectrum efficiency. In the experiments, 300 subcarriers and 225 subcarriers are used for B2B and 10-km MCF cases, respectively. In contrast, there is only ~ 5-dB of SNR variation of 2.5-km MCF within 30-GHz. This is because of the chirp induced spectral broadening of VCSEL. It means that to some extent the positive chromatic dispersion of the MCF compensates the chirps of VCSEL [24]. Thus, bit-power loading does not help much and 16QAM with 330 subcarriers are used for 2.5km MCF demonstration.

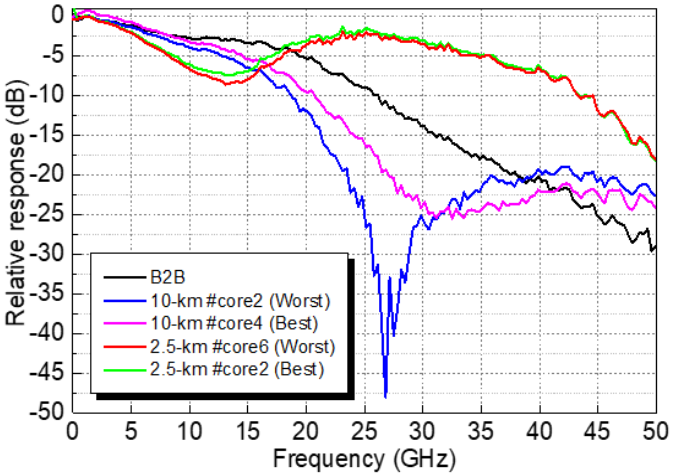

IV. Results and Discussions

In this section, first, the performance of optical B2B transmission case is demonstrated to show the optimization process of the nonlinearity tolerant DSP flow for optical DMT. After that, the transmission performance over 2.5-km and 10-km 7-core fibers is shown, respectively.

A. Optical B2B Performance Optimization

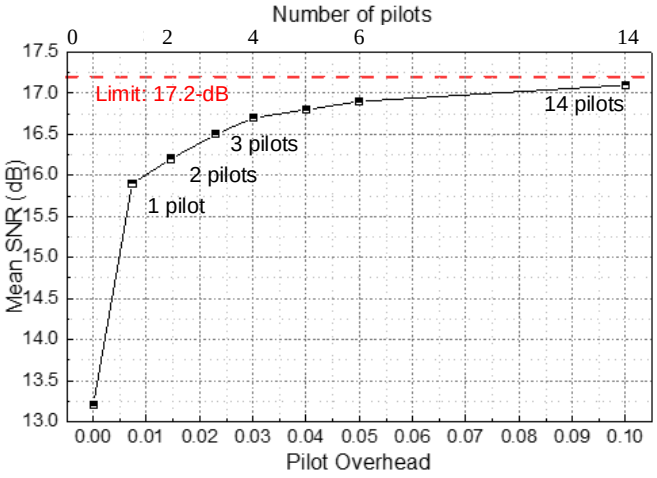

Fig. 7. Mean SNR versus pilot overhead for linear equalization.

The performance of the one-tap LE versus the LE pilot overhead is first demonstrated and shown in Fig. 7. The

received optical power (RoP) is 7-dBm. The performance limit of LE is calculated by treating all the DMT symbols as pilots. It can be seen that the mean SNR is improved by ~ 2.8-dB with only one pilot, and the performance is improved gradually by increasing the number of pilots. Finally, with 10% pilots overhead, the SNR can be improved by ~4-dB. In the experiments, we choose 5% pilots overhead (7 pilots) for LE as a trade-off between performance and system overhead.

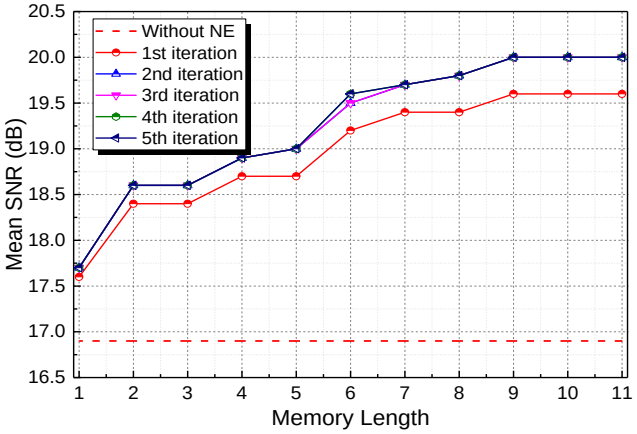

Fig. 8. Mean SNR versus memory length with iterations

The optimization of the NE is carried out after LE. The mean SNR under different memory lengths and after different iterations in the optical B2B case is shown in Fig. 8. The number of training symbols and the delay factor α are set as 8 and 3 respectively. The SNR without NE is also shown for comparison. With increased memory length, the mean SNR obviously improves. This is because more nonlinear kernels are considered in (5) resulting in a larger reduction of the nonlinear distortion. The SNR improvement by NE saturates when the memory length is larger than 9. Besides, the SNR is also improved with the process of NE iterations. There is a large improvement of SNR between the first and the second iteration, but the increment in SNR gain diminishes after 3 iterations, illustrating that the RLS algorithm has converged to the optimal achievable solution. With 3 iterations and a memory length of 9, a SNR gain of ~3.1-dB is achieved by NE. In the experiments, we choose memory length of 9 and iteration number of 4 for the NE to get the best transmission performance.

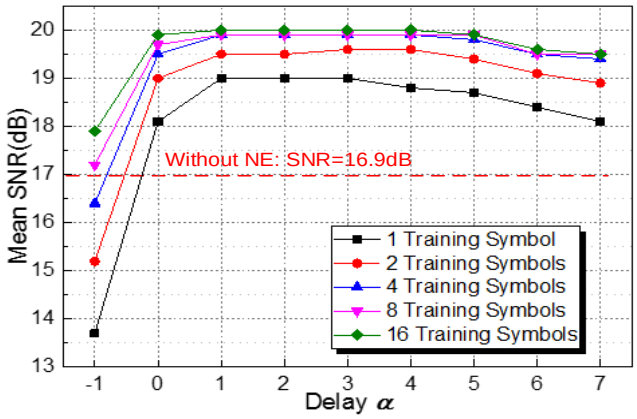

Fig. 9. Mean SNR versus delay factor and the number of training symbols

The impact of the delay factor α and the number of training symbols on the performance of the NE is also experimentally investigate and shown in Fig. 9. The SNR improvement by NE saturates when the number of training symbols exceeds 4, indicating that the training overhead of the nonlinearity tolerant DSP is limited. The optimal range of α is 1~3 regardless of the actual number of training symbols. In the experiments, we choose 4 training symbols and delay factor α of 3 for NE.

The SNR at the receiver is probed using a 16-QAM modulated DMT signal with 300 modulated subcarriers and shown in Fig. 10. The average SNR of the B2B case is 13.16-dB and it is improved to 16.87-dB after LE and further improved to 20-dB after NE. The channel equalization improves the mean SNR with ~ 7-dB. Compared to the measured system frequency response, it can be seen that the system response can be well recovered after LE and NE.

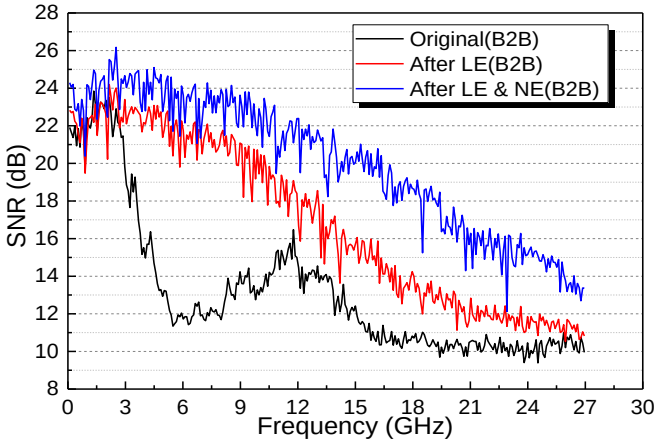

Fig. 10. Probed SNR versus frequency for optical B2B case

The spectrally-shaped channel is shown in Fig. 10, where the SNR is lower at high subcarrier frequencies. Adaptive bits and power loading is used to further increase the system capacity. The bits and power loading profiles of optical B2B transmission based on the probed SNR are shown in Fig. 11. More bits are allocated at low frequency region because of high SNR and more power are allocated at high frequency region to compensate the channel loss.

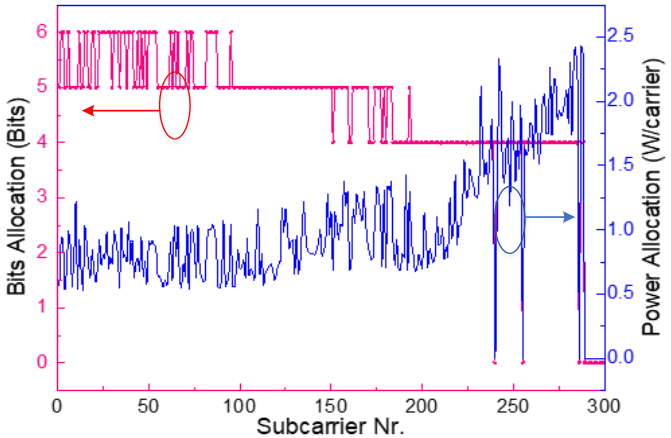

Fig. 11. Bits and power loading profiles at optical B2B transmission

The transmission performance of optical B2B case is shown in Fig. 12. The measured BER in function of the RoP at the PD input is shown in Fig. 12(a). It can be seen that the performance

after NE is significantly improved compared to the ones without any equalization or with only LE. The constellation graphs (i.e., without any equalization, with only LE and with both LE and NE) are shown in the insets (b)-(d) of Fig. 12. The BER lower than the threshold of the 7% HD-FEC of 3.8E-3 [25] is achieved with NE. For B2B, the achieved net data rate is 106.9-Gbit/s with bit and power loading and 94.2-Gbit/s without bit and power loading.

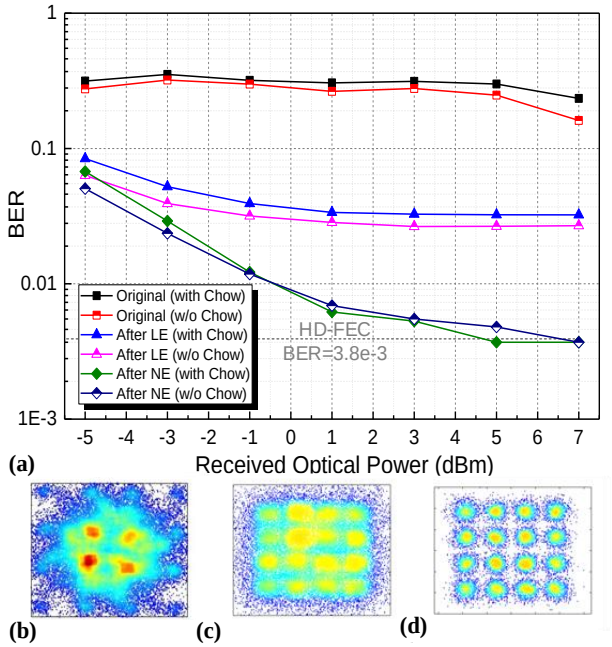

Fig. 12. (a) Performance comparison: BER versus RoP with various equalizations, (b) constellation diagram without any equalization, (c) with LE and (d) with both LE and NE.

B. 2.5-km and 10-km MCFs Transmission Performance

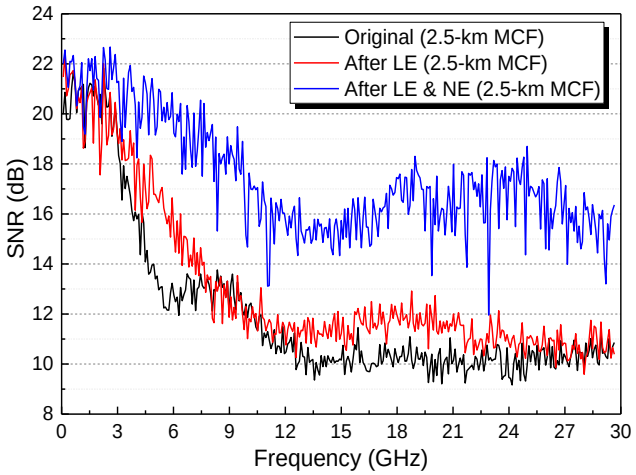

Fig. 13. Probed SNR versus frequency for 2.5-km MCF (the worst core)

The probed SNR of the worst core (core #6) of 2.5-km MCF is shown in Fig. 13. The average SNR of 2.5-km MCF transmission is 12.1-dB and it is improved to 13.1-dB after LE and to 17.4-dB after NE. The channel equalization improves the mean SNR with ~ 5-dB. Thus, NE is effective in compensating the link nonlinearities, which otherwise cause inter-subcarrier mixing. However, since the channel is not a typical spectrally-shaped channel according to the observation in Fig. 6 and the variation of SNR is severe, bits and power loading is not adopted for 2.5-km MCF case.

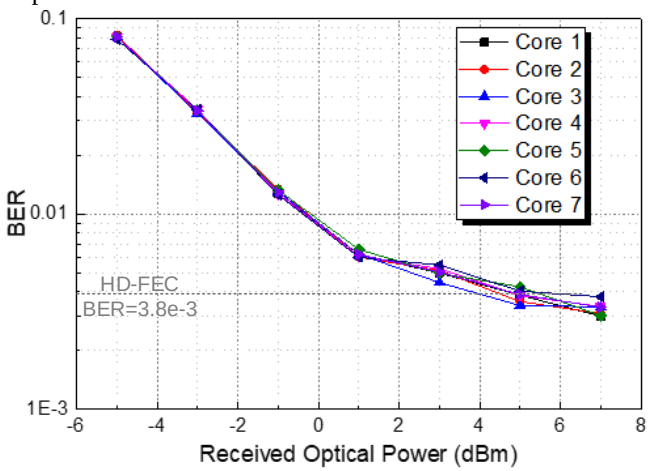

Fig. 14. BER versus RoP of 2.5-km MCF case.

The transmission performance of 2.5-km 7-core MCF case is shown in Fig. 14. A BER lower than the threshold of the 7% HD-FEC of 3.8E-3 for all 7 cores is achieved with NE. For 2.5-km MCF transmission. By adjusting the subcarrier numbers slightly, we have achieved gross-rates of 110.9-Gbit/s, 112.3-Gbit/s, 112.3-Gbit/s, 109.3-Gbit/s, 110.9-Gbit/s, 110.9-Gbit/s, and 110.9-Gbit/s at 7 different cores, respectively. Thus, the total system capacity with 2.5-km 7-core MCF is 777.5-Gbit/s (net-rate 726.6-Gbit/s).

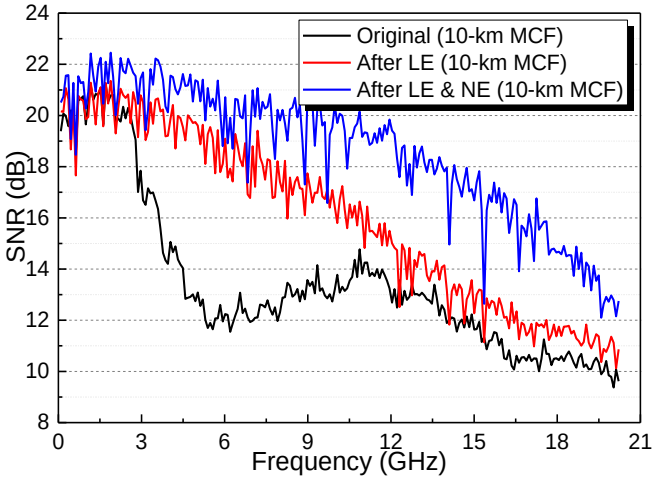

Fig. 15. Probed SNR versus frequency for 10-km MCF (the worst core)

The probed SNR of the worst core (core #2) after 10-km MCF transmission is shown in Fig. 15. The average SNR of 10-km MCF transmission is 13.4-dB and it is improved to 16.0-dB after LE and 18.6-dB after NE. The channel equalization improves the mean SNR with ~ 5-dB. Since the channel is a typical spectrally-shaped channel, bits and power loading is adopted for 10-km MCF case.

The transmission performance of 10-km 7-core MCF case is shown in Fig. 16. The BER lower than the threshold of the 7% HD-FEC of 3.8E-3 for all 7 cores are achieved with NE. For 10-km MCF transmission without bits and power loading, we have achieved gross-rates of 75.6-Gbit/s, 75.6-Gbit/s, 73.2-

Gbit/s, 75.6-Gbit/s, 77.3-Gbit/s, 73.2-Gbit/s, and 73.2-Gbit/s at 7 different cores, respectively. It leads to the total system capacity is 524.1-Gbit/s (net-rate 490.3-Gbit/s). For 10-km MCF transmission with bits and power loading, we have achieved better results, i.e., gross-rates of 88.3-Gbit/s, 77.1-Gbit/s, 76.4-Gbit/s, 88.9-Gbit/s, 80.2-Gbit/s, 75.1-Gbit/s, and 84.5-Gbit/s at 7 different cores, respectively. Thus, the total system capacity is improved to 570.5-Gbit/s (net-rate 533.1-Gbit/s).

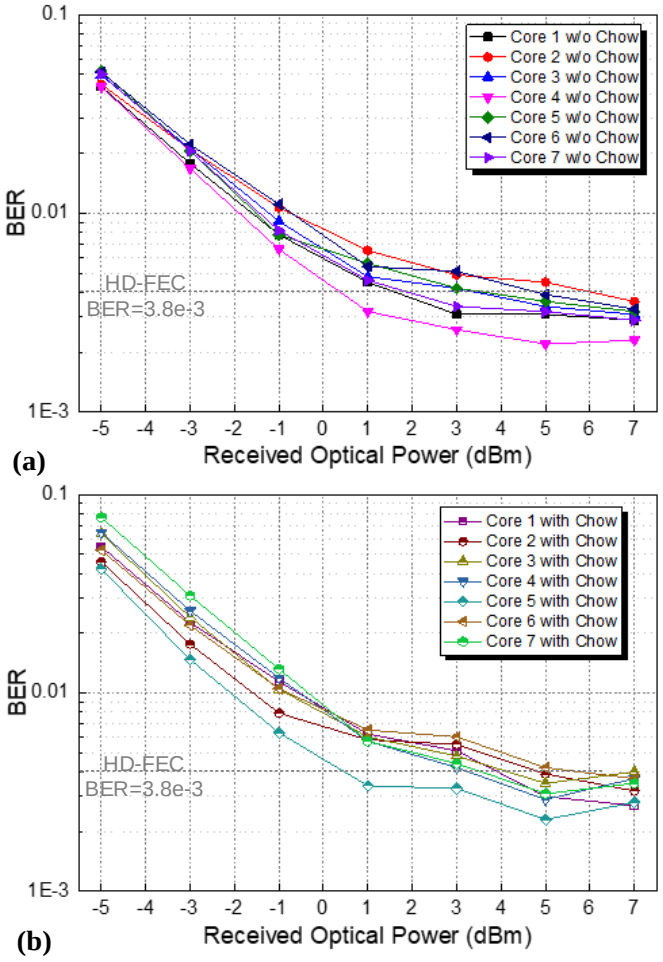

Fig. 16. (a) BER versus RoP of 10-km MCF case without Chow, (b) BER versus RoP of 10-km MCF case with Chow.

TABLE. I.
ACHIEVED NET DATA RATES WITH 2.5-KM/10-KM 7-CORE MCFS.

	Core Nr.	Net Data Rate (Gbit/s)							
		#1	#2	#3	#4	#5	#6	#7	Total
2.5-km MCF		103.7	105.0	105.0	102.1	103.6	103.6	103.6	**726.6**
10-km MCF	w/o Chow	70.9	70.9	68.5	70.7	72.3	68.5	68.5	**490.3**
	with Chow	82.5	72.1	71.4	83.1	74.9	70.1	79.0	**533.1**

V. CONCLUSIONS

In this paper, we have experimentally demonstrated nonlinearity tolerant high-speed optical DMT transmission over 2.5-km and 10-km 7-core MCFs using a 1.5-μm SM-VCSEL, with direct modulation bandwidth of 22-GHz. By employing nonlinearity tolerant DSP flow, the mean SNR has been improved by more than 5-dB compared with the system without channel equalization. The achieved net data rates are summarized in table. I. To the best of our knowledge, this is the highest DMT net-rate ever achieved by means of LW SM-VCSEL technology, which is a promising candidate to address the capacity challenges for future high-speed and cost-effective datacenter networks. Besides, since DMT is one of the multicarrier modulation schemes, which shares similar signal processing flow with modulation for mobile communications (e.g. OFDM), the proposed scheme also provides a high-speed solution for future mobile (e.g. 5G) access networks, such as analog radio-over-fiber systems.

REFERENCES

[1] Cisco global cloud index: forecast and methodology, 2015–2020. [Online]. Available: http://www.cisco.com/c/dam/en/us/solutions/collateral/service-provider/global-cloud-index-gci/white-paper-c11-738085.pdf

[2] IEEE P802.3bs 200 Gb/s and 400 Gb/s Ethernet task force. [Online]. Available: http://www.ieee802.org/3/bs/index.html

[3] D. Kuchta, "High-capacity VCSEL links," in *Proc. OFC*, Los Angeles, CA, USA, Mar. 2017, paper. Tu3C.4.

[4] R. Puerta, M. Agustin, Ł. Chorchos, J. Tońsk, J.-R. Kropp, Jr. N. Ledentsov, V.A. Shchukin, N.N. Ledentsov, R. Henker, I. Tafur Monroy, J.J. Vegas Olmos and J.P. Turkiewicz, "107.5 Gb/s 850 nm multi- and single-mode VCSEL transmission over 10 and 100 m of multi-mode fiber," in *Proc. OFC*, Anaheim, CA, USA, Mar. 2016, paper. Th5B.5.

[5] K. Fotini, S. Nebojsa, P. Cristian, Q. Zhang, and D. Thomas, "112 Gb/s PAM-4 optical signal transmission over 100-m OM4 multimode fiber for high-capacity data-center interconnects," in *Proc. ECOC*, Düsseldorf, Germany, Sep. 2016.

[6] T. Zuo, L. Zhang, J. Zhou, Q. Zhang, E. Zhou, and G. N. Liu, "Single lane 150-Gb/s, 100-Gb/s and 70-Gb/s 4-PAM transmission over 100-m, 300-m and 500-m MMF using 25-G class 850nm VCSEL," in *Proc. ECOC*, Düsseldorf, Germany, Sep. 2016.

[7] B. Wu, X. Zhou, Y. Ma, L. Jun, S. Qiu, K. Zhong, Z. Feng, C. Lu, S. Vitaly, K. Joerg, and L. Nikolay, "Single-lane 112Gbps transmission over 300m OM4 multimode fiber based on a single-transverse-mode 850nm VCSEL," in *Proc. ECOC*, Düsseldorf, Germany, Sep. 2016.

[8] C. Kottke, C. Caspar, V. Jungnickel, R. Freund, M. Agustin, and N. N. Ledentsov, "High speed 160 Gb/s DMT VCSEL transmission using pre-equalization," in *Proc. OFC*, Los Angeles, CA, USA, Mar. 2017, paper. W4I.7.

[9] S. Spiga, W. Soenen, A. Andrejew, D. M. Schoke, X. Yin, J. Bauwelinck, G. Boehm, and M. C. Amann, "Single-mode high-speed 1.5-µm VCSELs," *J. Light. Technol.*, vol. 35, no. 4, pp. 727-733, Aug. 2017.

[10] X. Yin, M. Verplaetse, L. Breyne, J. Van Kerrebrouck, T. De Keulenaer, A. Vyncke, R. Pierco, R. Vaernewyck, S. Spiga, M. -C. Amann, J. Chen, G. Van Steenberge, G. Torfs, and J. Bauwelinck, "Towards efficient 100 Gb/s serial rate optical interconnects: A duobinary way," in *Proc. OI*, Santa Fe, NM, USA, Jun. 2017, pp. 33-34.

[11] C. Xie, P. Dong, S. Randel, D. Pilori, P. Winzer, S. Spiga, B. Kögel, C. Neumeyr, M.C. Amann, "Single-VCSEL 100-Gb/s short-reach system using discrete multi-tone modulation and direct detection," in *Proc. OFC*, Los Angeles, CA, USA, Mar. 2015, paper. Tu2H.2.

[12] N. Eiselt, H. Griesser, J. Wei, R. Hohenleitner, A. Dochhan, M. Ortsiefer, M. H. Eiselt, C. Neumeyr, J. J. V. Olmos, and I. T. Monroy, "Experimental demonstration of 84 Gb/s PAM-4 over up to 1.6 km SSMF using a 20-GHz VCSEL at 1525 nm," *J. Light. Technol.*, vol. 35, no. 8, pp. 1342-1349, Feb. 2017.

[13] A. Dochhan, N. Eiselt, R. Hohenleitner, H. Griesser, M. Eiselt, M. Ortsiefer, C. Neumeyr, J. J. V. Olmos, I. T. Monroy, and J.-P. Elbers, "56 Gb/s DMT transmission with VCSELs in 1.5 um wavelength range over up to 12 km for DWDM intra-data center connects," in *Proc. ECOC*, Düsseldorf, Germany, Sep. 2016.

[14] M. Li, B. Hoover, V.N. Nazarov, and D.L. Butler, "Multicore fiber for optical interconnect applications," in *Proc. OECC*, Busan, South Korea, Jul. 2012. pp. 564-565.

[15] A. Larsson, P. Westbergh, J.S. Gustavsson, E. Haglund, and E.P.Haglund, "High-speed VCSELs and VCSEL arrays for single-and multi-core fiber interconnects," in *Proc. SPIE OPTO*, San Francisco, CA, USA, Mar. 2015,

vol. 9381, pp. 93810D-1.
[16] J. Van Kerrebrouck, L. Zhang, R. Lin, X. Pang, A. Udalcovs, O. Ozolins, S. Spiga, M. C. Amann, G. Van Steenberge, L. Gan, M. Tang, S. Fu, R. Schatz, S. Popov, D. Liu, W. Tong, S. Xiao, G. Torfs, J. Chen, J. Bauwelinck and X. Yin, "726.7-Gb/s 1.5-μm single-mode VCSEL discrete multi-tone transmission over 2.5-km multicore fiber," in *Proc. OFC*, San Diego, CA, USA, Mar. 2018, paper. M1I.2.
[17] B. Li, Z. Feng, M. Tang, Z. Xu, S. Fu, Q. Wu, L. Deng, W. Tong, S. Liu, and P. P. Shum, "Experimental demonstration of large capacity WSDM optical access network with multicore fibers and advanced modulation formats," *Opt. Express.*, vol. 23, no. 9, pp. 10997-11006, Feb. 2015.
[18] J. Tu, K. Saitoh, M. Koshiba, K. Takenaga, and S. Matsuo, "Design and analysis of large-effective-area heterogeneous trench-assisted multi-core fiber," *Opt. Express.*, vol. 20, no. 14, pp. 15157–15170, Jun. 2012.
[19] F. Barrami, Y. L. Guennec, E. Novakov, and P. Busson, "Impact of VCSEL nonlinearity on discrete MultiTone modulation: Quasi-static approach," In *Proc. ICT*, Lisbon, Portugal, May. 2014, pp. 113-118
[20] P. S. Chow, J. M. Cioffi, and J. A.C. Bingham, "A Practical Discrete Multitone Transceiver Loading Algorithm for Data Transmission over Spectrally Shaped Channels", *IEEE Trans. Commun.*, vol. 43, no. 234, pp. 773-775, Apr. 1995.
[21] L. Zhang, S. Xiao, M. Bi, L. Liu, and Z. Zhou, "Channel estimation algorithm for interference suppression in IMDD–OQAM–OFDM transmission systems," *Opt. Commun.*,vol 364, pp. 129-133, Apr. 2016.
[22] X. Hong, O. Ozolins, C. Guo, X. Pang, J. Zhang, J. R. Navarro, A. Kakkar, R. Schatz, U. Westergren, G. Jacobsen, S. Popov, and J. Chen, "1.55-μm EML-based DMT Transmission with Nonlinearity-Aware Time Domain Super-Nyquist Image Induced Aliasing," in *Proc. OFC*, Los Angeles, CA, USA, Mar. 2017, paper Th3D.3.
[23] L. Zhang, X. Hong, X. Pang, O. Ozolins, A. Udalcovs, R. Schatz, C. Guo, J. Zhang, F. Nordwall, K. M. Engenhardt, U. Westergren, S. Popov, G. Jacobsen, S. Xiao, W. Hu and J. Chen, "Nonlinearity-aware 200-Gbit/s discrete multi-tone transmission for C-band short-reach optical interconnects with a single packaged EML," *Opt. Letters.*, vol. 43, no. 2, pp. 182-185, Jan. 2018.
[24] J. Van Kerrebrouck, H. Li, S. Spiga, M. C. Amann, X. Yin, J. Bauwelinck, P. Demeester and G. Torfs, "10 Gb/s Radio-Over-Fiber at 28 GHz Carrier Frequency Link Based on 1550 nm VCSEL Chirp Enhanced Intensity Modulation after 2 km Fiber," in *Proc. OFC*, San Diego, CA, USA, Mar. 2018, paper. W1F.1.
[25] ITU -T Recommendation G.975.1, 2004, Appendix I.9.